Depth-dependent rheology and the horizontal length scale of mantle convection

A. Lenardic,[1] M. A. Richards,[2] and F. H. Busse[3]

Received 21 January 2005; revised 20 September 2005; accepted 16 January 2006; published 25 July 2006.

[1] Numerical simulations show that depth-dependent viscosity can increase the wavelength of mantle convection. The physical mechanism behind this phenomenon and its robustness with respect to model parameters remain to be fully elucidated. Toward this end, we develop theoretical heat flow scalings for a convecting fluid layer with depth-dependent viscosity. Bottom and internally heated end-members are considered. For the former, the viscosity structure consists of a high-viscosity central region bounded from above and below by horizontal low-viscosity channels. For internally heated cases, only a surface low-viscosity channel is present. Theoretical scalings derived from boundary layer theory show that depth-dependent rheology lowers the lateral dissipation associated with steady state convective rolls, allowing longer aspect ratio cells to form as the viscosity contrast between the channels and the central region is increased. The maximum cell aspect ratio is estimated from the condition that the pressure gradients that drive lateral flow in the channels do not become so large as to inhibit vertical flow into the channels. Scaling predictions compare favorably to results of numerical simulations for steady state cells. As the Rayleigh number driving convection is increased, small-scale boundary layer instabilities begin to form. This increases lateral dissipation within the channels and the preferred cell aspect ratio decreases as a result. Internally heated simulations show that a near-surface high-viscosity layer, an analog to tectonic plates, can suppress these small-scale instabilities. This allows a low-viscosity channel to maintain large aspect ratio cells for Rayleigh numbers approaching that of the present-day Earth.

Citation: Lenardic, A., M. A. Richards, and F. H. Busse (2006), Depth-dependent rheology and the horizontal length scale of mantle convection, *J. Geophys. Res.*, *111*, B07404, doi:10.1029/2005JB003639.

1. Introduction

[2] Plate motions at the Earth's surface represent a highly unusual style of thermal boundary layer motion in response to solid-state thermal convection in the deep mantle. This style is apparently unique in the solar system, at least at the present time. Among the unique features are nearly piecewise-constant surface velocities over distances that far exceed the depth of convection (e.g., the Pacific plate), as well as phenomena such as whole plate subduction and stable ridge-transform systems; none of these features are found in convection studies of normal fluids.

[3] Diverse rheological mechanisms must be responsible for plate-style convection on Earth. Temperature dependence of viscosity alone leads ultimately to a "stagnant lid" style of convection [e.g., *Solomatov*, 1995], which may, for example, explain the current convective regime of Mars [*Schubert et al.*, 1992]. However, lithospheric failure (faulting) is also necessary for plate formation, and considerable attention has been devoted recently to both theoretical and numerical modeling of mantle convection with various failure mechanisms or nonlinear rheologies [*Bercovici*, 1996; *Moresi and Solomatov*, 1998; *Tackley*, 1998; *Trompert and Hansen*, 1998]. These studies reveal a complicated variety of behavior, including episodic overturning with limited periods of plate-like behavior [*Moresi and Solomatov*, 1998], which may, for example, explain some aspects of tectonics on Venus [*Turcotte*, 1993]. More interestingly, truly stable plate-like behavior does occur when a strong, "breakable" lithosphere is combined with the existence of a very weak zone beneath the lithosphere; a consistent finding among several recent and related numerical modeling studies [*Tackley*, 2000a, 2000b; *Richards et al.*, 2001; *Stein et al.*, 2004].

[4] Since the discovery of plate tectonics four decades ago, geophysicists have suspected, and often assumed, that a low viscosity layer beneath the lithospheric plates may play a central role in facilitating plate motions. This notion derives from a much longer-standing body of geophysical evidence for a mechanically weak "asthenosphere" [e.g., *Anderson and Sammis*, 1970; *Craig and McKenzie*, 1986], as well as perhaps an intuitive sense that plates must be "lubricated" in order to allow them to move intact. Over the past two decades geodynamic studies of the geoid and postglacial rebound have been interpreted to require the

[1]Department of Earth Science, Rice University, Houston, Texas, USA.
[2]Department of Earth and Planetary Science, University of California, Berkeley, California, USA.
[3]Institute of Physics, University of Bayreuth, Bayreuth, Germany.

0148-0227/06/2005JB003639$09.00

upper mantle be 1–2 orders of magnitude less viscous, on average, than the lower mantle, and it is quite possible that most of this variation might be confined to the uppermost sublithospheric mantle [*Hager and Richards*, 1989; *Thoraval and Richards*, 1997]. Seismological evidence [e.g., *Gutenberg*, 1959] has long suggested that a sublithospheric channel of low-velocity exists beneath much of the oceanic lithosphere, but not beneath stable continental lithosphere, consistent with the fact that the plate tectonic model itself is based largely on the behavior of large oceanic plates. The origin of the seismic low-velocity zone is controversial [e.g., *Stixrude and Lithgow-Bertelloni*, 2005], but it may be due to straightforward pressure effects on constituent mineral elastic properties, or to more exotic effects arising from partial melting and the presence of volatile components, i.e., water [*Karato and Jung*, 1998].

[5] A number of geodynamic modeling studies have focused on the possible role of a low-viscosity zone (LVZ) in plate tectonics and mantle convection, and these studies do indeed point to important dynamic effects. For example, it has been known for some time that an LVZ may lead to larger aspect ratio convection cells than normally occur in isoviscous convection [*Richter and Daly*, 1978; *Jaupart and Parsons*, 1985]. Numerical convection simulations, incorporating depth-dependent viscosity, have confirmed that viscosity stratification can have a first-order effect on the planform of mantle convection [*Hansen et al.*, 1993; *Zhang and Yuen*, 1995]. Recent studies indicate that this effect is quite pronounced. *Bunge et al.* [1996, 1997] explored internally heated, 3-D spherical convection models at moderate (10^6) Rayleigh number in which the viscosity of the upper mantle was a factor of 20–30 lower than that of the lower mantle, and found dramatic effects on planform that exceed other likely effects, such as modest degrees of bottom (core) heating and phase changes. In these models, viscosity stratification converts the planform from an almost white spectrum of point-like downwellings to a very red spectrum of sheet-like downwellings. *Tackley* [1996a] examined 3-D models of mantle convection with strongly temperature-dependent viscosity, and found similarly strong effects on planform. Of particular note is that *Tackley* [1996a] found that almost all the effect on convection planform can be attributed to the horizontally averaged viscosity structure. *Zhong et al.* [2000] and *Zhong and Zuber* [2001] also explored the role of a depth variable viscosity on numerical simulations of mantle convection and confirmed that a low viscosity upper mantle, above a higher-viscosity lower mantle, significantly increases the wavelength of mantle convection compared to simulations lacking depth-dependent viscosity.

[6] Thus it appears that radial viscosity stratification of the mantle can explain various lines of evidence [e.g., *Su and Dziewonski*, 1992] that mantle convection occurs at significantly longer wavelengths than one would normally expect at mantle Rayleigh numbers approaching 10^8, where horizontal structures usually occur at wavelengths considerably less than the depth of the convecting fluid (mantle). The general conclusion from numerical modeling studies that radial viscosity stratification, especially an LVZ, leads to longer-wavelength and more stable convection planform also appears consistent with recent findings that an LVZ promotes stable, plate-like convection [*Richards et al.*, 2001]. Indeed, it seems reasonable to infer that Venus lacks plate tectonics because it lacks an LVZ, as evidenced from gravity/topography admittance studies [*Kiefer et al.*, 1986; *Kaula*, 1990].

[7] Given its likely importance in determining the nature of mantle convection and plate tectonics on Earth, one would hope to be able to derive a clear, physical understanding of the effect of an LVZ on convection that would lead to further insights and, perhaps, testable theoretical predictions. However, we are unaware of any studies that offer a straightforward fluid mechanical explanation for why an LVZ should promote plate motions, or how vertical viscosity stratification affects mantle convection in general. We believe that obtaining such an understanding should lead to a more fundamental understanding of plate tectonics on Earth as well as mantle convection in the other terrestrial planets. Such is the goal of the theoretical analysis and numerical results presented in this paper, and our emphasis is on explaining stable, long-wavelength structure at moderate to high Rayleigh number.

[8] We use a modification of established boundary layer theory to formulate a simple physical analysis of the effect of an LVZ on heat flow and the horizontal scale for convection. We then test the predictions of this analysis with 2-D numerical models of convection, demonstrating good agreement. We then explore numerical models in which an LVZ is overlain by a strong (''lithospheric'') layer, and find that the effect of the LVZ is much enhanced in this configuration, which we believe is relevant to the origins of plate tectonics.

2. Analysis and Numerical Simulations

[9] Although the criteria that determine the selection of convective planforms within a thermally convecting fluid are not generally understood [e.g., *Ahlers*, 1995], it is agreed that lateral dissipation can limit the formation of large aspect ratio cells [*Busse*, 1985]. For convective onset, it has already been shown that viscosity stratification can shift the neutral stability curve toward longer wavelength by lowering lateral dissipation [*Richter and Daly*, 1978]. That is, long-wavelength flow becomes favored at the onset of convection for fluids with depth-dependent viscosity [*Jaupart and Parsons*, 1985]. However, if the degree of viscosity stratification becomes too great, convection can become confined to the low-viscosity region and, as a result, short-wavelength cells are predicted to occur at convective onset [*Buffett et al.*, 1994]. The cited work applies only to small amplitude flow just past convective onset. It is not clear how this carries over to the case of fully developed, finite amplitude convection of the type that occurs in the Earth's mantle. We will show that depth-dependent viscosity can lower lateral dissipation in fully developed, large amplitude convective flow systems heated from below or from within. This shifts the limit on the maximum cell aspect ratio that is energetically favorable. That is, with depth-dependent viscosity, the cell wavelength that is most effective at transporting heat is longer than for the isoviscous case. Although this does not guarantee that long cells will form preferentially to shorter cells, it does show how

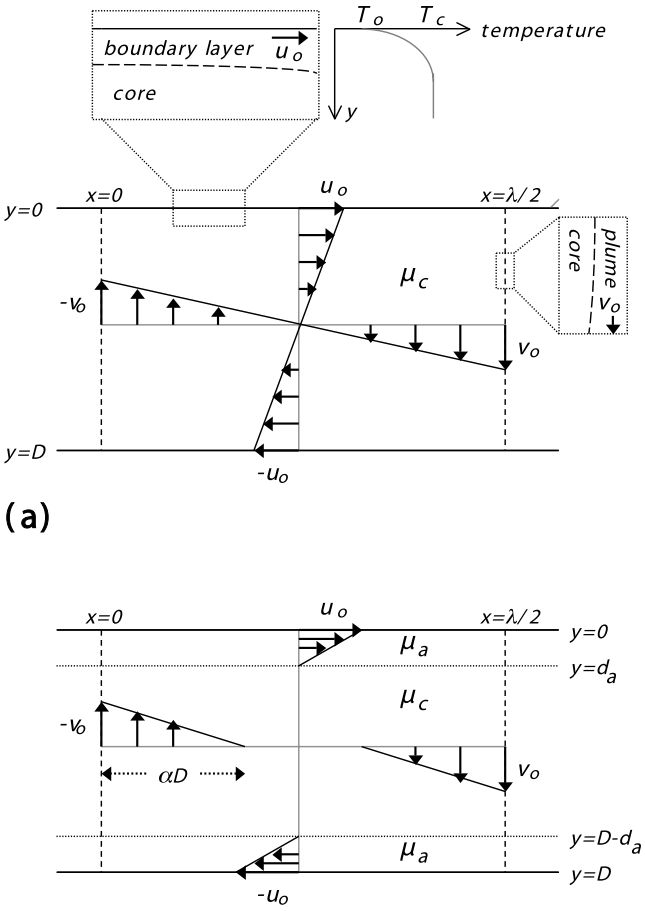

Figure 1. (a) Cartoon of convective cell structure for constant viscosity convection. (b) Cartoon of convective cell structure for convection with low-viscosity channels.

depth-dependent viscosity can make this more favorable by maximizing heat transport.

2.1. Bottom Heating, Double-Channel End-Member

[10] The relationship between heat flow and cell length for steady state convection rolls in an isoviscous, bottom heated fluid has been addressed using boundary layer theory [*Turcotte and Oxburgh*, 1967; *Turcotte and Schubert*, 1982]. Our analysis is a straightforward variation on this approach (Figure 1). As such, a short review of the basic ideas behind boundary layer theory will be useful as will results for the isoviscous case.

[11] Boundary layer theory assumes that the Rayleigh number, *Ra*, driving convection is much greater than the value for convective onset so that horizontal thermal boundary layers and sinking/rising vertical plumes are thin relative to the system depth, *D* (Figure 1a). Convection cells are dominated by a central core region where motions are driven by shear stresses imposed by vertical plumes and horizontal boundary layers. In this limit, the internal cell temperature, T_c, is the average of the surface, T_0, and base temperature, T_1. Flow velocities in plumes and boundary layers are considered to be spatially constant, and flow in the central region of the cell can be approximated, to first-order, as being composed of linear velocity profiles as shown in Figure 1a. The rate at which work is done on the plumes by gravitational body forces must equal the rate at which work is done on the boundaries by viscous forces. Together with a statement of mass conservation, this work balance allows the nondimensional heat flux, i.e., the Nusselt number, *Nu*, to be solved for as a function of *Ra* and the aspect ratio of convection cells, $\lambda/(2D)$. The expression is given by [*Turcotte and Schubert*, 1982]

$$Nu = \frac{1}{2^{1/3}\pi^{2/3}} \frac{\left(\frac{\lambda}{2D}\right)^{2/3}}{\left[1+\left(\frac{\lambda^4}{16D^4}\right)\right]^{1/3}} Ra^{1/3}. \quad (1a)$$

The $\lambda^4/16D^4$ term in the denominator of equation (1a) represents lateral dissipation, and it is this dissipation that leads to the prediction that large aspect ratio cells will be inefficient at transporting heat. The aspect ratio that is most effective at transporting heat, at a fixed *Ra*, can be solved for using equation (1a) and is found to be

$$\frac{\lambda}{2D} = 1. \quad (1b)$$

[12] The lack of an aspect ratio-dependent vertical dissipation term in the denominator of equation (1a) results from the fact that the simple theory described above assumes that the length scale of vertical shear can increase continually with increasing aspect ratio (Figure 1a). This is clearly an over simplification since for very large aspect ratio cells the extent of the vertical shear layer should not greatly exceed the depth of the system, *D*. In effect, this simplification limits the applicability of the analysis to cell aspect ratio's not much greater than unity. It has already been shown that beyond the aspect ratio at which the vertical shear scale becomes constant, increasing aspect ratio will lead a decrease in the efficiency of heat transport regardless of how low the lateral dissipation becomes [*Grigné et al.*, 2005]. That is, beyond the aspect ratio at which the vertical shear scale becomes constant, lateral dissipation is no longer the principal limit on convective efficiency. Rather, it is vertical dissipation that limits the extent of convection cells beyond this point. We will return to this point below.

[13] We now consider the effects of allowing for horizontal channels of thickness *d* and viscosity μ_a that bound a central region of viscosity μ_c (Figure 1b). Both μ_a and μ_c are considered to be very large relative to the thermal diffusivity of the fluid (i.e., infinite Prandtl number flow). The system is characterized by the thickness of the channels, the Rayleigh number, *Ra*, defined in terms of the system depth and central viscosity, and the viscosity ratio $\mu_r = \mu_a/\mu_c$. We again assume convection to be in the form of steady state rolls, and that thermal boundary layers are thin relative to *D* and *d*. We assume that lateral flow becomes channelized within the low viscosity regions and consider the first-order approximation of linear velocity profiles as shown in Figure 1b. Flow channelization is the key difference between the boundary layer analysis for the system of Figure 1b versus 1a. It affects the lateral dissipation of the system and alters the form of the mass conservation equation. We have also shown in Figure 1b a maximum

horizontal extent of the vertical shear scale which we denote as a multiple of the system depth, β D, were β is of the order of one. The theory developed will assume that the vertical shear scale increases linearly with aspect ratio up to this maximum shear scale. Thereafter, the theory is not expected to be valid. The maximum vertical shear scale factor β will not be constrained by the simple theory we develop but will be constrained using numerical simulations (we note that higher-order theory can be developed that predicts the horizontal structure [*Busse et al.*, 2006; *Morris*, 2005]). Aside from this limitation on the maximum aspect ratio for which the theory is valid and the assumption of flow channelization, the analysis will follow classical boundary layer theory [*Turcotte and Oxburgh*, 1967; *Turcotte and Schubert*, 1982].

[14] The main principle of boundary layer theory is that the rate at which work is done on sinking/rising plumes by gravitational body forces must equal the rate at which work is done on the boundaries of the interior region of a convection cell by viscous forces. To determine the viscous contribution, the horizontal shear stress due to the lateral motion of thermal boundary layers, τ_h, and the vertical shear stress due to sinking/rising plumes, τ_v, must be known. For the system of Figure 1b these shear stress terms are given by

$$\tau_h = \mu_a \frac{2u_0}{d} \tag{2}$$

and

$$\tau_v = \mu_c \frac{4v_0}{\lambda}, \tag{3}$$

where we have assumed that $d \ll D$. The vertical and horizontal velocities are related through the statement of mass conservation expressed as

$$\frac{v_0 \lambda}{2} = u_0 d. \tag{4}$$

Notice that the expressions for the isoviscous case can be retrieved by setting $d = D$ and $\mu_a = \mu_c$. Expressing the downward gravitational body force on one-half of a symmetrical plume as F_b, the statement of work balance can be written as

$$2F_b v_0 = 2D\tau_v v_0 + \lambda \tau_h u_0. \tag{5}$$

The expression for F_b follows from classic boundary layer theory [*Turcotte and Schubert*, 1982] and is given by

$$F_b = 2\rho_0 g \alpha D (T_c - T_0) \frac{u_0}{v_0} \left(\frac{\kappa \lambda}{2\pi u_0} \right)^{1/2}, \tag{6}$$

where ρ_o is the reference density, g is gravitational acceleration, α is the coefficient of thermal expansion, and κ is the thermal diffusivity. The symmetry of the system of Figure 1b allows us to express the isothermal internal temperature of the convection cell, T_c, in terms of fixed surface and base temperatures as

$$T_c = T_0 + \frac{T_1 - T_0}{2}. \tag{7}$$

We can combine equations (2)–(7) to derive an expression for the mean horizontal velocity along the upper boundary of the cell, u_0. The expression is given by

$$u_0 = \frac{\kappa}{D} \frac{\left(\frac{d}{D}\right)^{2/3} \left(\frac{\lambda}{2D}\right)^{7/3}}{\left[\left(\frac{d}{D}\right)^3 + \left(\frac{\lambda^4}{16D^4}\right) \frac{\mu_a}{\mu_c}\right]^{2/3}} \left(\frac{Ra}{2\sqrt{\pi}} \right)^{2/3}, \tag{8}$$

where $Ra = \rho_0 g \alpha (T_1 - T_0) D^3 / (\kappa \mu_c)$. Notice that this velocity increases as the viscosity ratio between the channels and the central cell region, $\mu_r = \mu_a / \mu_c$, decreases. This can be tracked back to the expression for the horizontal shear stress (equation (2)), and it highlights a key distinction between the systems of Figures 1b and 1a. Notice also that in the limit of μ_r tending toward zero, the horizontal velocity increases as d/D decreases. This can be tracked back to the continuity equation (equation (4)) and is a consequence of flow channelization into low-viscosity regions.

[15] We can use equation (8) to solve for the system heat flow. The total rate of heat flow, Q, out of the convection cell per unit distance along the cell axis is given by

$$Q = 2k(T_c - T_0) \left(\frac{u_0 \lambda}{2\pi\kappa} \right)^{1/2}, \tag{9}$$

where k is the thermal conductivity [*Turcotte and Oxburgh*, 1967; *Turcotte and Schubert*, 1982]. Inserting equation (8) and nondimensionalizing by the heat flow that would occur by conduction in the absence of convection leads to an expression for the Nusselt number given by

$$Nu = \frac{1}{2^{1/3}\pi^{2/3}} \frac{\left(\frac{d}{D}\right)^{1/3} \left(\frac{\lambda}{2D}\right)^{2/3}}{\left[\left(\frac{d}{D}\right)^3 + \left(\frac{\lambda^4}{16D^4}\right) \mu_r\right]^{1/3}} Ra^{1/3}. \tag{10a}$$

The key difference between equations (10a) and (1a) is that the term associated with lateral dissipation is multiplied by μ_r in equation (10a). This occurs because, for the system of Figure 1b, lateral dissipation is associated with flow in the low viscosity channels. The aspect ratio that is most effective at transporting heat at a fixed Ra can be solved for using equation (10a) and is found to be

$$\frac{\lambda}{2D} = \left[\frac{(d/D)^3}{\mu_r} \right]^{1/4}. \tag{10b}$$

Notice that this aspect ratio increases with decreasing μ_r and the simple physical explanation for this is that the lateral dissipation in the system decreases with decreasing μ_r. Notice also from equation (10a) that for fixed aspect ratio in the limit of μ_r tending toward zero, the system heat flux increases as d/D decreases. This is due to the fact that the horizontal velocity must increase as d/D decreases, all other factors remaining fixed, in order to satisfy mass conservation.

[16] An equivalent, energy dissipation based analysis, to that provided above, is also given by *Richards et al.* [2003] and *Morris* [2003]. The simplified assumptions with regard to velocity profiles means that this analysis is not expected to be quantitatively exact. However, predicted trends should be robust. Specifically, equation (10a) predicts that for the limit of μ_r tending toward zero, the Nusselt number should scale as $(\lambda/2D)^{2/3}$ as long as the vertical shear scale, βD, continues to increase with increasing aspect ratio. Similarly, although equation (10b) is not expected to provide the exact value of the aspect ratio that maximizes heat flux, the prediction that this aspect ratio should increase with decreasing μ_r should be robust.

[17] An alternate analysis can bring added clarity to the physical meaning of equation (10b) [*Richards et al.*, 2003; *Morris*, 2003]. Flow in the low-viscosity channels requires a horizontal pressure gradient. long-wavelength cells will become unstable when the pressure gradient forces in the channels approach the vertical shear forces acting on the central region. If the pressure gradient force becomes too large, fluid from the central region of the cell will not be able to enter the channels and channelized flow, as in Figure 1b, will not occur. The pressure gradient can be estimated by balancing horizontal flux in the channels with vertical flux in the central region of the cell. The result is

$$\frac{\partial p}{\partial x} = \frac{3}{2}\frac{v_0 \mu_a}{d^3}\frac{\lambda}{2}. \tag{11a}$$

The pressure gradient force acting on a channel is given by $\frac{1}{2}(\partial p/\partial x)(\lambda/2)^2$, while the vertical shear force acting on the central region of the cell is given by $(2v_0\mu_c D)/(\lambda/2)$. Balancing these two terms leads to

$$\frac{\lambda}{2D} = \left[\frac{8}{3}\frac{(d/D)^3}{\mu_r}\right]^{1/4}, \tag{11b}$$

which, aside from a constant, is equivalent to equation (10b).

[18] That two different approaches lead to an equivalent form of the expression for the maximum cell wavelength is particularly important. The derivation of equation (10b) is based on an energetic argument. To use it as a criterion for determining the cell aspect ratio that will be favored in nature amounts to invoking an optimal type theory, i.e., the cell aspect ratio that forms will be the one that is energetically most efficient [e.g., *Howard*, 1972; *Busse*, 1978]. A long-standing objection to optimal theories is that they do not provide any mechanism as to why the system should evolve toward the efficient state. The pressure gradient based argument leading to equation (11b) shows that for the particular problem we are addressing, the energetically optimal condition is of the same form as a condition based on a simple force balance. This provides a physical mechanism for the system moving toward the optimal state, i.e., force imbalances will drive flow toward a balanced state.

[19] To test the validity of the scaling trends, we undertook a suite of numerical simulations. The CITCOM finite element code was used. Its accuracy in treating convection problems involving large viscosity gradients has been documented [*Moresi and Solomatov*, 1995; *Moresi et al.*, 1996] and we performed our own convergence testing for our specific application to assure that simulations were well resolved. Thermal boundary conditions for simulations in this section are constant surface and basal temperatures of, respectively, zero and one, with adiabatic side walls. Mechanical boundary conditions are free slip at all boundaries.

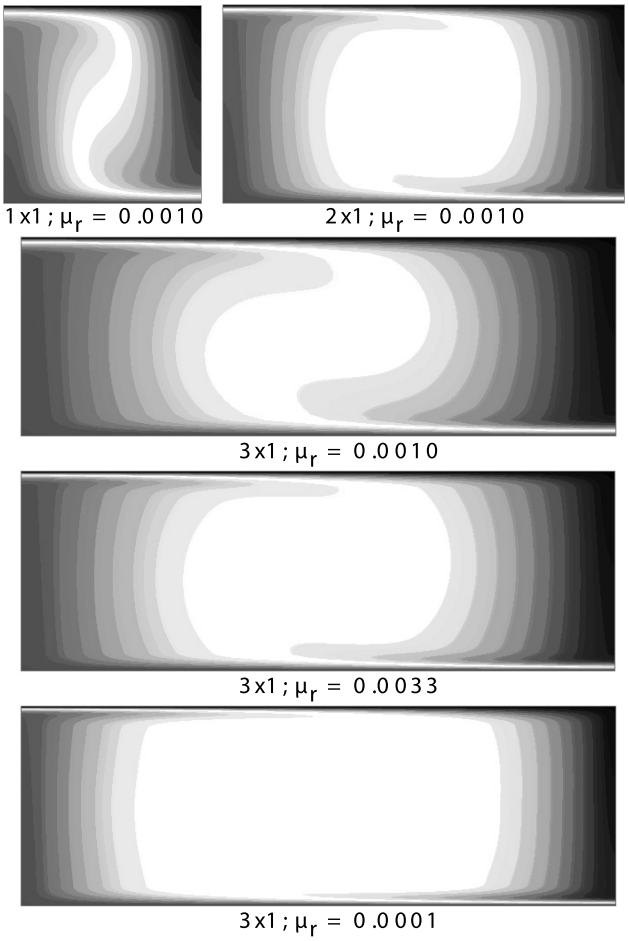

Figure 2. Thermal fields from bottom heated numerical simulations.

[20] Simulation suites explored the dependence of *Nu* on cell aspect ratio. For each suite, all parameters were held fixed except for the modeling domain width. The initial condition was a fixed wavelength perturbation from the conductive state. The wavelength of the perturbation was set such that for any aspect ratio domain, it would generate a single, box filling cell. After any single simulation was run for several system overturn times the simulation was stopped and restarted with a short-wavelength perturbation to test the stability of the long-wavelength cell. Figure 2 shows thermal fields from representative steady state cases. Notice that as the viscosity ratio increases, lateral flow becomes focused into the channels in accord with our theoretical assumption (Figure 1b).

[21] Figure 3 shows representative vertical velocity profiles at the middepth of simulation cells. The vertical velocity profiles constrain the maximum horizontal extent of vertical shear that occurs adjacent to thermal upwellings

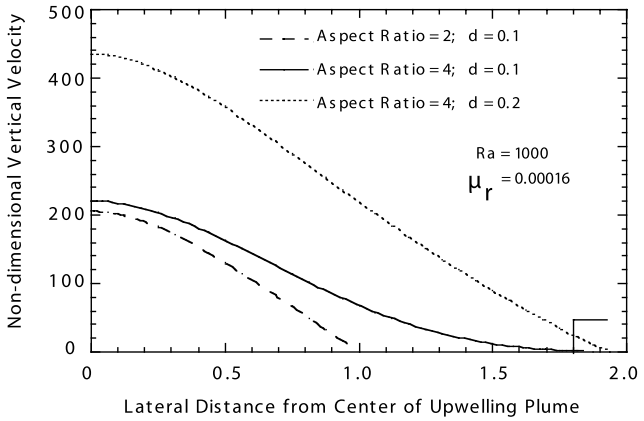

Figure 3. Nondimensional vertical velocity versus the lateral extent from the center of an upwelling plume for simulations with different aspect ratios and channel thicknesses. The velocity plots show the extent of the vertical viscous shear layer that forms adjacent to thermal upflows and downflows.

and downwellings. Notice that for the thinner channel cases the extent of the vertical shear layer increases with increasing aspect ratio and that the maximum extent is about 1.5 times the system depth. This implies that the theory developed should be valid up to aspect ratio's of 3 (subject to the assumed values of *Ra*, *d*, and μ_r). Notice also that the horizontal extent of vertical shear is a function of the channel thickness. The theory we have developed does not address this dependence.

[22] Figure 4a plots the results from several simulation suites in terms of *Nu* and cell aspect ratio together with the theoretically predicted trend based on equation (10a) in the limit of $\mu_r \ll 1$. The theoretical trend is shown only out to an aspect ratio of 3 as the horizontal extent of vertical shear does not increase with aspect ratio beyond this point for the simulations shown. The fact that the numerical curves roll over before this aspect ratio is reached implies that even for the most extreme viscosity variation models, lateral dissipation provides a limit on the efficiency of heat transfer. The simulations confirm that the cell aspect ratio that maximizes heat flux increases with decreasing μ_r. The scaling predicted *Nu* versus cell aspect ratio trend, up to the maximizing cell extent, is also in accord with simulation results. Figure 4b plots the effects of channel thickness on *Nu* for simulations that are in the limit of $\mu_r \ll 1$. The scaling prediction that *Nu* should increase with decreasing channel thickness (equation (10a)) is consistent with simulation results (Figure 4b). The deviation from the predicted scaling trend for thick channels is expected as our theory assumes $d \ll D$. The deviation for thin channels is also expected as the thickness of thermal boundary layers approaches the thickness of the channels, which moves the thin channel simulations out of the applicability range of our theory. Nonetheless, even for the thin channel cases, the prediction that heat flux increases with decreasing channel thickness is seen to remain valid (Figure 4b).

[23] Figure 5a plots the aspect ratio that maximizes heat flux determined from simulation suites together with the theoretically predicted trends based on equations (10b) and (11b). Although qualitative predictions are consistent with simulation results, the quantitative fit is poor. Simple boundary layer analysis of the type we have followed assumes a linear dependence on x of the vertical velocity in the cell interior (Figure 1). As already noted, for large aspect ratio cells this assumption becomes overly simplified as, with increasing aspect ratio, the stress exerted by the vertical plumes should become confined to a distance much smaller than $\lambda/4$ from the plumes. A more detailed analysis that accounts for this can be applied to our problem [*Busse et al.*, 2006; *Morris*, 2005]. That analysis solves for the horizontal extent of vertical shear as a function of system parameters, leading to the following higher-order scaling

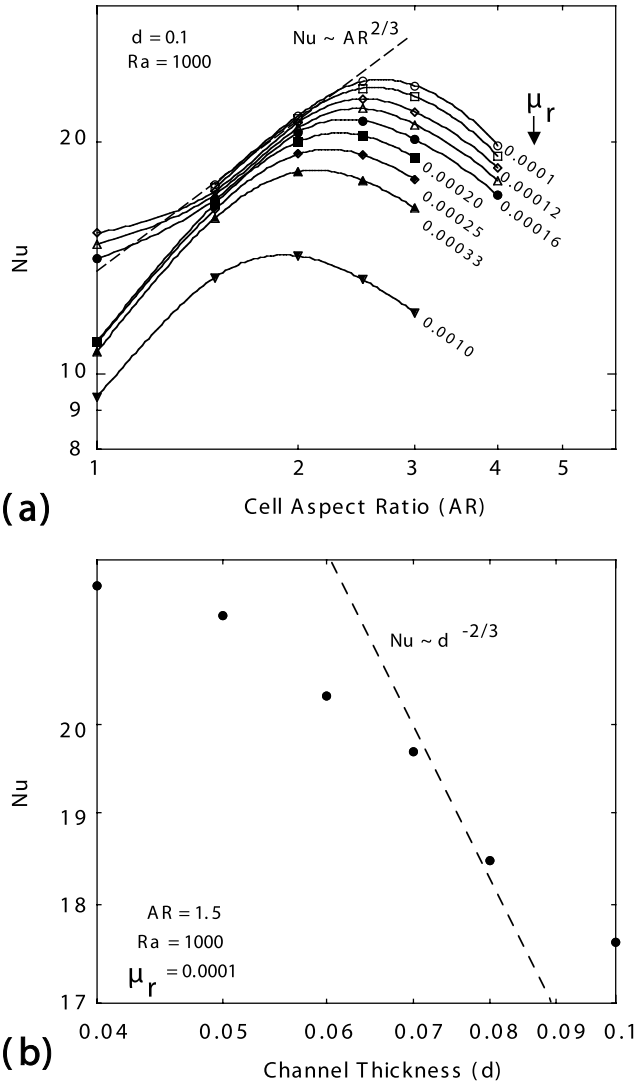

Figure 4. (a) Numerical simulation results for the Nusselt number, *Nu*, as a function of cell aspect ratio compared to theoretically predicted trend. (b) Numerical simulation results for the *Nu* as a function of channel thickness, *d*, compared to theoretically predicted trend. The noted Rayleigh number, *Ra*, is defined using the central core viscosity.

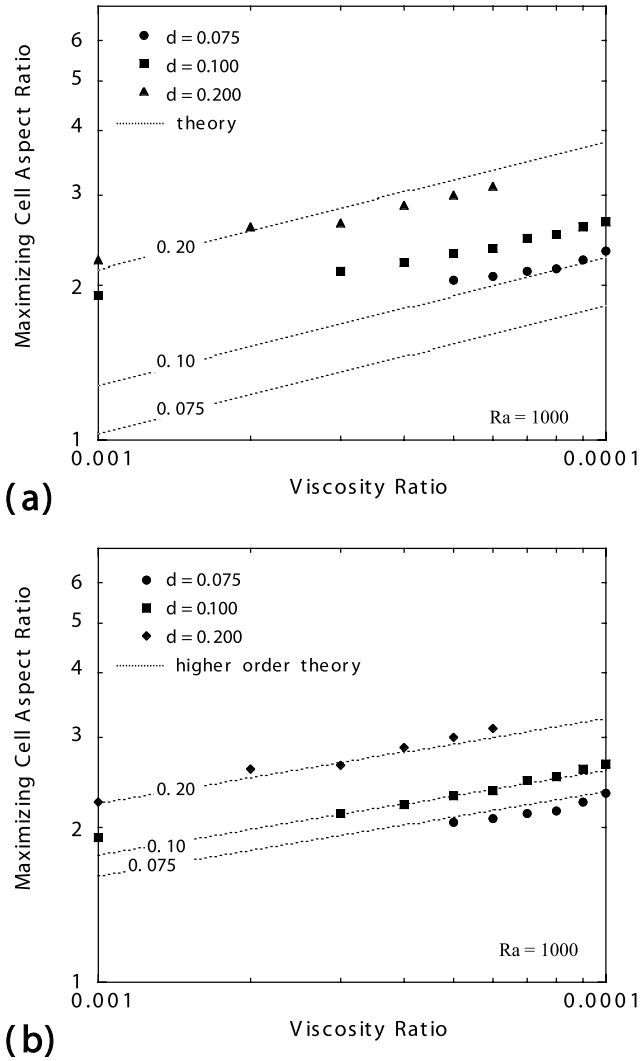

Figure 5. (a) Numerical simulation results for the *Nu*-maximizing cell aspect ratio as a function of the viscosity ratio and channel thickness compared to theoretically predicted trends. (b) Numerical simulation results for the *Nu*-maximizing cell aspect ratio as a function of the viscosity ratio and channel thickness compared to predicted trends from a higher-order theory.

for the aspect ratio that is most effective at transporting heat:

$$\frac{\lambda}{2D} = \left(\pi 9^{-1/6}\right)\left[\frac{(d/D)^3}{\mu_r}\right]^{1/6}. \qquad (12)$$

Figure 5b shows that this corrected scaling provides a much improved fit to simulation results. The predictions that *Nu* should scale as the cell aspect ratio to the 2/3 power and should increase with decreasing *d*, in the limit of μ_r tending toward zero (equation (10a)), remain unchanged. Although the simplified analysis is clearly deficient relative to the higher-order analysis, it does capture qualitative trends and, unlike the more detailed analysis of *Busse et al.* [2006], it can easily be extended to address internally heated convection, as will be discussed in section 2.2.

[24] Figure 6 shows the effects of increasing *Ra*. Unlike the cases in Figure 4a, the higher *Ra* cases of Figure 6 are time-dependent. These cases were run to a statistically steady state and plotted Nusselt numbers are temporally averaged mean values. That a statistically steady state was achieved was confirmed by monitoring the Nusselt number and RMS velocity from each simulation. Simulation time series were averaged after the initial start up phase using variable averaging windows. A simulation was considered to have entered a statistically steady state when averages determined from increasing time duration windows differed by less than 2–3%. A total energy balance was also monitored as a double check. Heat flow into the base of the system and out of the system were monitored to assure that the system, as a whole, was not heating or cooling over the time frame for which average output values where determined.

[25] Figure 6 shows that the onset of time dependence, with increasing *Ra*, leads to a decrease in the extent of a cell that maximizes heat flow. For the highest *Ra* cases, a peak in the *Nu* curves becomes very weak. For higher *Ra* cases than shown, cell aspect ratios significantly greater than unity could not be stabilized (i.e., long cells broke down into shorter cells before a statistically state was achieved). This confirms previous observations, based on numerical simulations, that increasing *Ra* leads to shorter-wavelength flow in mantle convection models with depth-dependent rheology [*Tackley*, 1996a, 1996b]. It should be stressed that our theoretical scalings do not break down simply because *Ra* is high; indeed, boundary layer theory relies on high *Ra*. The breakdown of the theory is due instead to the onset of time dependence which alters the flow profiles within the low viscosity channels, i.e., the assumed flow profiles of Figure 1b are no longer valid. Figure 7 shows that time

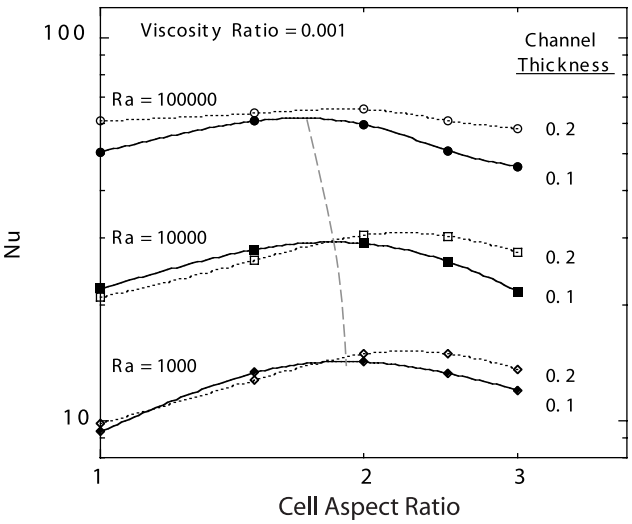

Figure 6. (a) Numerical simulation results for *Nu* as a function of cell aspect ratio for simulations with increased *Ra*. The dashed grey line shows that the maximizing aspect ratio decreases with increasing *Ra*.

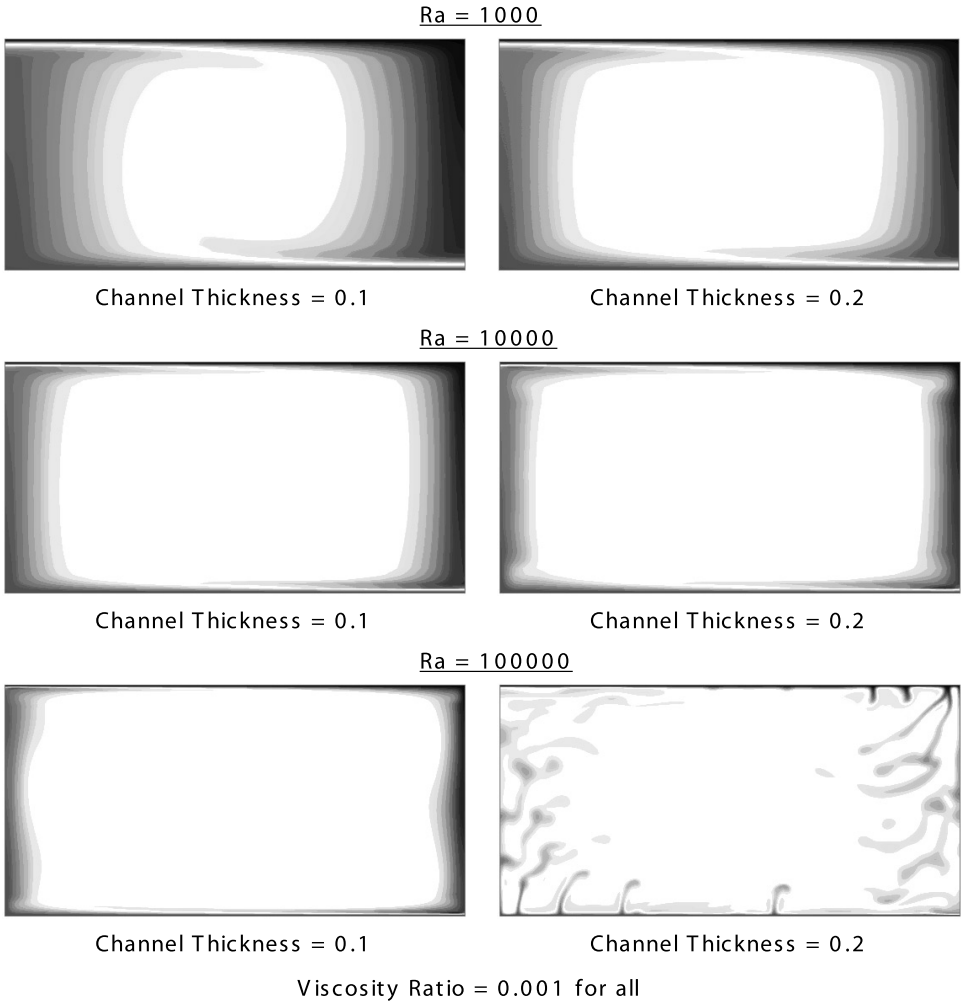

Figure 7. Thermal fields from bottom heated numerical simulations with increased *Ra*.

dependence is associated with small-scale boundary layer instabilities. These instabilities generate large velocity gradients within the channel, causing an increase in lateral dissipation. Our analysis showed that low lateral dissipation is what allows for relatively long wavelength cells, and it is thus expected that increased dissipation will shift convection toward shorter wavelength. The distinction between increased *Ra* versus the onset of boundary layer instabilities causing our theory to breakdown is not just one of semantics. It suggests that if a mechanism for suppressing boundary layer instabilities at higher *Ra* exists, then long wavelength flow could occur at higher *Ra* values. This issue is taken up in section 2.2.

2.2. Internal Heating End-Member

[26] For internally heated convection, energetic efficiency cannot be assessed by considering surface heat flux as was the case for bottom heating. Instead the average temperature rise across the convecting layer, compared to its value if heat were removed by conduction, is used to assess efficiency. The temperature rise across the convecting layer is given by the internal temperature within the cell minus the fixed surface temperature, $T_c - T_0$. For a layer with uniform heat production per unit mass of H, density of ρ, thermal conductivity of k, and a depth of D, the temperature rise across the layer if conduction removed all heat would be $\rho HD^2/2k$. The ratio of the temperature rise with convection divided by the value without convection is denoted by θ, and the smaller this ratio the more efficient convection is in cooling the interior of the fluid. For an isoviscous layer, classic boundary layer theory can be used to derive a relationship between θ, the internally heated Rayleigh number, Ra_i, and the cell aspect ratio, $\lambda/2D$ [*Turcotte and Schubert*, 1982]. The relationship is given by

$$\theta = (2\pi)^{1/2} \frac{\left[1 + \left(\frac{\lambda^4}{16D^4}\right)\right]^{1/4}}{\left(\frac{\lambda}{2D}\right)^{1/2}} Ra_i^{-1/4}. \tag{13a}$$

The $\lambda^4/16D^4$ term in the numerator of equation (13a) represents lateral dissipation and, analogous to the bottom heated case, long aspect ratio cells are not efficient at cooling the interior because they are associated with large dissipation. The aspect ratio that is most effective at cooling the interior, at a fixed Ra_i, can be solved for using equation (13a) and is found to be

$$\frac{\lambda}{2D} = 1. \tag{13b}$$

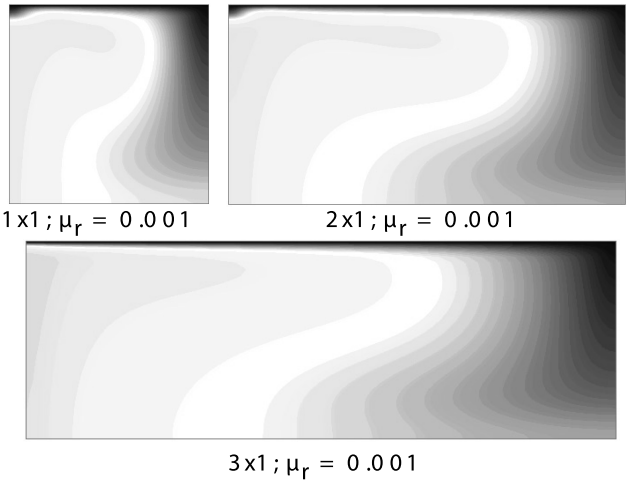

Figure 8. Thermal fields from internally heated numerical simulations with a surface low-viscosity channel. For the smaller aspect ratio cases, small-scale corner rolls formed above the main broad thermal upflow as can be seen in the top left corner of the thermal images for the 1×1 and 2×1 simulations. These stable corner rolls did not form for larger aspect ratio cases.

[27] We now consider the effects of allowing for a horizontal channel of thickness d and viscosity μ_a above an underlying "central" region of viscosity μ_c. The Rayleigh number, Ra_i, is again defined in terms of the system depth and central viscosity. We again consider convection to be in the form of steady state rolls with lateral flow channelized within the low viscosity surface channel. The first-order approximation of linear velocity profiles is retained as per section 2.1. As with the bottom heated case, the boundary layer analysis follows the classic analysis for an isoviscous layer except for the changes in the horizontal shear stress term and the mass conservation equation. Taking these changes into account within the boundary layer analysis leads to a relationship for θ given by

$$\theta = (2\pi)^{1/2} \frac{\left[\left(\frac{d}{D}\right)^3 + \left(\frac{\lambda^4}{16D^4}\right)\mu_r\right]^{1/4}}{\left(\frac{d}{D}\right)^{1/4}\left(\frac{\lambda}{2D}\right)^{1/2}} Ra_i^{-1/4}. \quad (14a)$$

Notice that as with the bottom heated case, the lateral dissipation term becomes multiplied by μ_r when a low-viscosity channel is introduced. This allows longer aspect ratio cells to be energetically efficient. The aspect ratio that is most effective at cooling the interior, at a fixed Ra_i, can be solved for using equation (14a) and is found to be

$$\frac{\lambda}{2D} = \left[\frac{(d/D)^3}{\mu_r}\right]^{1/4}. \quad (14b)$$

[28] Internally heated simulations were performed to test the validity of scaling predictions. Thermal boundary conditions for simulations of this section are a constant surface temperature of zero, an insulating base, and adiabatic sidewalls. Mechanical boundary conditions are free slip. Figure 8 shows thermal fields from representative steady state cases. Figure 9a shows results from several simulations suites in θ cell aspect ratio space. Notice that as the viscosity ratio decreases, the cell aspect ratio associated with greatest interior cooling increases as predicted by our scaling analysis. Additional simulation results showed that the internally heated scaling predictions maintained reasonable consistency with simulation results, provided the system remained in steady state. The degree of match between scaling prediction and simulation results was comparable to that of section 2.1 for bottom heated cases. As with bottom heated cases, scaling predictions broke down as Ra_i was increased (Figure 9a), and this was again due to the onset of time dependence and the consequent increase in lateral dissipation.

[29] Results presented thus far show that a low-viscosity channel has the potential to push mantle convection toward longer wavelengths by lowering the lateral dissipation

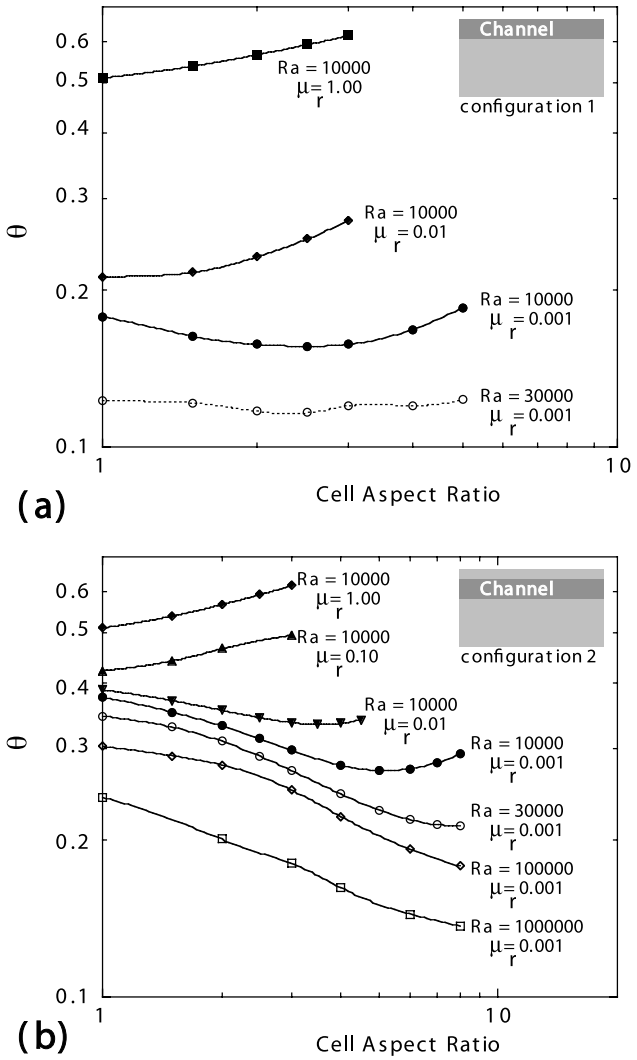

Figure 9. (a) Numerical simulation results for θ as a function of cell aspect ratio for internally heated convection with a near-surface low-viscosity channel. (b) Numerical simulation results for θ as a function of cell aspect ratio for internally heated convection with a submerged low-viscosity channel.

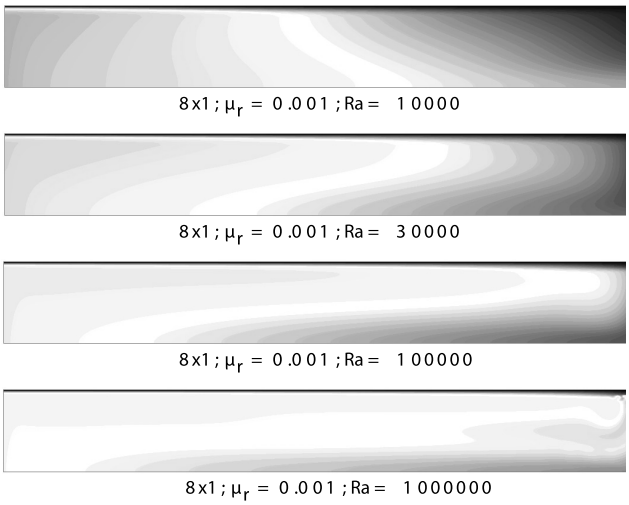

Figure 10. Thermal fields from internally heated numerical simulations with a submerged low-viscosity channel.

associated with plate movement. The applicability of this idea is, however, brought into question by the fact that our results also show a shift to shorter wavelength at Rayleigh numbers well below the Earth's present-day value [e.g., *Davies and Richards*, 1992]. We reemphasize that the shift is due to the onset of small-scale boundary layer instabilities that increase lateral dissipation. For the system we have explored thus far these instabilities arise at relatively low Rayleigh numbers because the upper boundary layer is assumed to have the same low viscosity as the low-viscosity channel. For Earth, the viscosity of the upper boundary layer, i.e., of the plates, will be much greater than that of the asthenosphere. This higher viscosity likely stabilizes the upper boundary layer and thus allow a low-viscosity channel to maintain long-wavelength flow at higher Rayleigh numbers. Our final set of simulations explores this possibility.

[30] We consider internally heated simulations in which the low viscosity channel does not extend to the surface of the modeling domain, as in the inset of Figure 9a but is instead "submerged" below a higher-viscosity layer, as in the inset of Figure 9b. Figure 9b shows results from several submerged channel simulations suites in θ cell aspect ratio space. Thermal fields from representative long-wavelength cases are shown in Figure 10. For all the suites the channel thickness is 0.1 and the channel is submerged a nondimensional distance of 0.05 from the surface of the domain. The near-surface layer of thickness 0.05 is a highly idealized analog of a tectonic plate. The viscosity of the surface layer and the interior region of the cell are equal for the simulations of Figures 8b and 9. This allows the surface layer to participate in convection, i.e., the layer remains active as opposed to stagnant.

[31] Comparison of the results shown in Figures 8a and 8b shows that the submerged channel, as compared to the surface channel, configuration allows long-wavelength cells to be efficient at cooling the interior at higher Rayleigh numbers. Simulations that varied the viscosity of the near-surface layer indicate that this conclusion does depend on the surface layer participating in convection (Figure 11). As the viscosity ratio of the surface layer relative to central core region increases, the velocity of the surface layer decreases and the surface layer itself becomes stagnant. A stagnant surface layer leads to a large velocity gradient from the base of the layer into the low-viscosity channel which increases lateral dissipation. This, in turn, makes long wavelength cells inefficient at cooling the interior, verifying the suspected mechanisms at play.

[32] Figures 9b and 10 suggest the need for a theoretical analysis exploring the interaction between a low-viscosity channel and high viscosity "plates," together with numerical simulations that sweep the full parameter space of the extended system. This goes beyond the scope of the present paper, but these preliminary results make it clear that "in the presence of a strong lithosphere" the effect of an LVZ in generating long-wavelength structure is preserved to higher *Ra* regimes than might otherwise occur.

3. Discussion

[33] The boundary layer analysis presented at the outset of this paper yields a straightforward physical explanation for why an LVZ promotes long-wavelength structure in finite amplitude convection. In normal viscously dominated convection, the horizontal length scale is limited by the rapid increase in horizontal shear dissipation that occurs as convection cells grow longer. Horizontal shear dissipation is markedly reduced by a thin, low-viscosity layer below (above) a cold (hot) boundary layer. Note that it would be misleading to attribute this effect to "lubrication" of the bottom of the boundary layer, because the effect we have explored does not occur for the simpler situation of a cold, stiff boundary layer overlying an otherwise isoviscous fluid interior.

[34] Our analysis predicts (equation (10a)) that *Nu* scales with the 2/3 power of convection cell length for sufficiently large viscosity contrasts, and this prediction is verified in

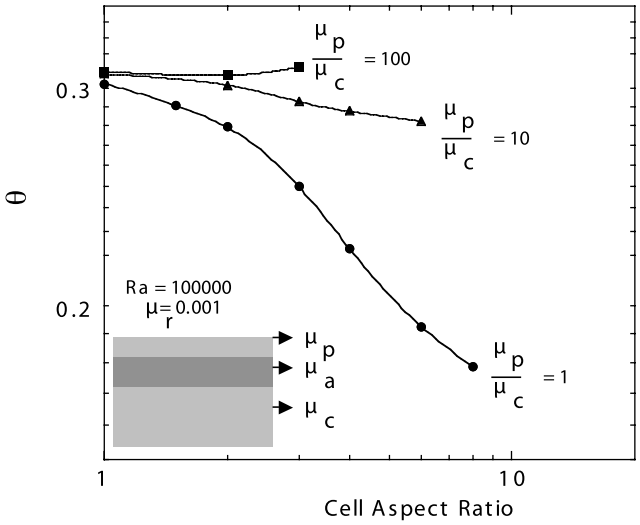

Figure 11. Numerical simulation results for θ as a function of cell aspect ratio for internally heated convection with a submerged low-viscosity channel and a variable surface layer viscosity.

numerical tests. Numerical tests also verify the theoretical prediction (equation (12)) for how the optimum cell length scales with channel thickness and viscosity contrast. A fuller theoretical analysis published elsewhere [*Busse et al.*, 2006; *Morris*, 2005] is necessary to obtain the correct scaling, because the less rigorous result (equation (10b)) does not adequately address the vertical viscous shear scale associated with thermal upwellings and downwellings.

[35] Equations (10a) and (12) thus constitute a simple theory for the effect of low-viscosity zones for the ''symmetric'' case of bottom heated convection. A similar theory (equations (14a) and (14b)) holds for internally heated convection (cold boundary layer underlain by a low viscosity channel), although the correct scaling for cell length has not yet been derived theoretically, and it is likely that equation (14b) should be replaced by an expression similar to equation (12). The analysis for the internally heated case is also verified by numerical modeling, suggesting that the full theoretical analysis of the symmetric case [*Busse et al.*, 2006] is indeed relevant to planetary mantle convection.

[36] As anticipated, these results have limited utility, in a strict sense, because they break down at the higher Rayleigh numbers applicable to mantle convection in the terrestrial planets. Short wavelength boundary layer instabilities at high *Ra* effectively introduce a great deal of horizontal shear dissipation, negating the ''advantage'' of longer convection cells afforded by an LVZ. Nevertheless, the modeling and analysis results summarized above led us to hypothesize that if the LVZ were ''submerged'' beneath a higher viscosity layer (''lithosphere''), as imposed by temperature-dependent viscosity in mantle convection, then the short-wavelength instabilities would be inhibited, and the LVZ effect on cell length might be restored. This is, in fact, exactly what is revealed in numerical tests (Figure 9b). The submerged LVZ results in a dramatic increase in the length of stable convection cells even at moderately high *Ra*. For viscosity contrasts of 1000 or more the preferred cell length appears almost unbounded, although our numerical models are limited by finite domain length. The numerical models show that *Nu* increases with decreasing channel thickness (for sufficiently strong viscosity contrast). The reason this happens is that as the LVZ becomes thinner, horizontal flow velocities within the low-viscosity channel increase, thereby increasing the efficiency of cooling at the base of the higher-viscosity thermal boundary layer (lithosphere). Altogether, these results demonstrate that an LVZ beneath a strong (but mobile) lithosphere will result in very long wavelength structure in convection, even at high *Ra*.

[37] Much work remains to be done to fully understand the lithosphere/LVZ interaction discussed above. However, we believe that the preliminary results of Figure 9b offer a straightforward explanation for why an LVZ is so effective in promoting a plate tectonic style of mantle convection: A combination of the reduction of shear dissipation, rapid horizontal channel flow due to the LVZ, and suppression of downwelling instabilities by a cold, relatively stiff lithosphere result in large aspect ratio cells with nearly piecewise-constant upper surface velocities. The caveat is that the upper thermal boundary layer can fail (fault) at a yield stress comparable to the characteristic stresses due to convection. This explanation is appears fully consistent with the recent numerically based findings of *Tackley* [2000a, 2000b], *Richards et al.* [2001], and *Stein et al.* [2004].

[38] The numerical models (both here and in the plate-like simulations) suggest that an LVZ must represent a viscosity contrast of 2–3 orders of magnitude in order to be effective in promoting long-wavelength structure and plate-like boundary layer motions. As noted in the Introduction, there is considerable independent geophysical evidence that the upper mantle has an average viscosity 1–2 orders of magnitude less than that of the lower mantle, depending upon how one parameterizes the mantle layers. The most robust constraints are from models of the geoid and postglacial rebound, but it is well known that there is little model resolution on the radial viscosity structure. For example, *Thoraval and Richards* [1997, Figure 5], exploring various geoid modeling trade-offs, showed that geoid constraints can be met with a low-viscosity layer between 80 and 220 km depth for viscosity contrasts of 1–4 orders of magnitude, depending upon other modeling parameters (especially the details of the lithospheric boundary condition!). It is less clear to us how forgiving postglacial rebound data may be in similar regards, but we know of no data that exclude either a ''thick,'' moderate-contrast LVZ filling most of the upper mantle or a ''thin,'' high-contrast layer corresponding roughly to the thickness of the seismic low-velocity zone.

[39] The results of this study do not depend on the particular physical mechanism(s) responsible for an LVZ on Earth, because the empirical geophysical constraints appear sufficient to warrant serious consideration in any case. The origin of the ''asthenosphere'' and *Gutenberg*'s [1959] low-velocity zone beneath oceanic lithosphere and tectonically active continental lithosphere remains a matter of long-standing controversy. *Stixrude and Lithgow-Bertelloni* [2005] argue that subsolidus mineralogical responses to increasing pressure may be sufficient to explain the seismic low-velocity zone without resort to partial melting or near saturation by volatile components. *Karato and Jung* [1998] suggest that subsolidus effects of water may also explain both the LVZ and the seismic low-velocity zone, due to the weakening effect of water on bond strengths in olivine and other constituent minerals. Certainly, if water is the culprit, then the implication that Venus lacks plate tectonics because it is dry is reinforced by the lack of evidence for an LVZ there [e.g., *Kiefer et al.*, 1986]. Yet another possibility is that lattice preferred orientation (LPO) in the uppermost mantle preferentially weakens the sublithospheric mantle, as suggested by evidence for seismic anisotropy in the upper mantle low-velocity zone beneath the Pacific Ocean [*Ekstrom and Dziewonski*, 1998].

[40] Our results also beg consideration of how an LVZ and, perhaps by implication, water in the upper mantle control, or are maintained by, feedback effects in the overall thermal and chemical evolution of terrestrial planets. Such questions are, of course, far beyond the scope of this study, but to the extent that we have reinforced the idea that the presence of an LVZ may be an essential element of plate tectonics on Earth, it becomes even more clear that geophysicists need to focus more on the fundamental nature of this region of the mantle.

[41] As a final note, the issue of long-wavelength convection extends beyond purely Earth-based interests. It has

been suggested that the Martian hemispheric dichotomy is the result of long-wavelength convection in the early Martian mantle coupling to the crust and causing it to thicken over one side of the planet [*McGill and Dimitriou*, 1990; *Zhong and Zuber*, 2001]. This has naturally led to the question of whether long-wavelength convection is likely to occur under the conditions that prevailed early in Mars' history. Our results suggest that depth-dependent rheology can allow for long-wavelength flow although they cannot confirm that this is likely at the high Rayleigh numbers that would prevail early in the history of a planet. Our results also suggest that the mantle lithosphere must have been mobile to allow for long wavelength flow in early Mars (Figure 11). A degree of mobility for the mantle portion of the lithosphere is also required if the dichotomy did indeed form as a result of mantle convection driven crustal thickening. Lithospheric mobility can be achieved if Mars was in a sluggish lid mode of convection early in its history or if it experienced an early episode of plate tectonics [*Sleep*, 1994; *Nimmo and Stevenson*, 2000; *Lenardic et al.*, 2004].

4. Conclusions

[42] Theoretical boundary layer analysis, combined with numerical simulations, demonstrate how low-viscosity layers within a convecting mantle can lead to a flow channelization that lowers the lateral dissipation associated with convection cells. This allows larger aspect ratio cells to form as the ratio of channel to bulk mantle viscosity decreases. This result is shown to hold for both bottom and internally heated convection. Small-scale boundary layer instabilities, which arise when the Rayleigh number becomes sufficiently large, disrupt the channel flow and increase lateral dissipation. As a result, long-wavelength cells become unstable once boundary layer instabilities appear. A high viscosity, mobile surface layer above a lower-viscosity channel can suppress the onset of boundary layer instabilities and allow flow channelization to maintain long-wavelength convection cells for Rayleigh numbers approaching the Earth's present-day value. Collectively, our results suggest that the Earth's asthenosphere plays a crucial role in determining the characteristic length scale of mantle convection. They also offer an explanation for why an LVZ may represent an essential requirement for plate tectonics.

[43] **Acknowledgments.** This work was begun as a collaboration among the coauthors and Stephen Morris, who declined to be a coauthor on this paper. We thank Stephen for fruitful discussions and his insights into the formulation of the stability criterion for the bottom-heated case. We also thank C. Grigne, S. Labrosse, and P. J. Tackley for helpful discussions regarding their own work and its relationship to the ideas expressed within this paper. The quality of this paper was improved by the constructive reviews of two anonymous referees and the Associate Editor. The work documented has been supported by NASA-MDAP grant NAG5-12166 and NSF grant EAR-0448871.

References

Ahlers, G. (1995), Over two decades of pattern formation, a personal perspective, in *25 Years of Nonequilibrium Statistical Mechanics*, edited by J. J. Brey et al., pp. 91–124, Springer, New York.

Anderson, D. L., and C. Sammis (1970), Partial melting in the upper mantle, *Phys. Earth Planet. Inter.*, *3*, 41–50.

Bercovici, D. (1996), Plate generation in a simple model of lithosphere-mantle flow with dynamic self-lubrication, *Earth Planet. Sci. Lett.*, *144*, 41–51.

Buffett, B. A., C. W. Gable, and R. J. O'Connell (1994), Linear stability of a layered fluid with mobile surface plates, *J. Geophys. Res.*, *99*, 19,885–19,900.

Bunge, H. P., M. A. Richards, and J. R. Baumgardner (1996), Effect of depth-dependent viscosity of the planform of mantle convection, *Nature*, *379*, 436–438.

Bunge, H. P., M. A. Richards, and J. R. Baumgardner (1997), A sensitivity study of 3-dimensional spherical mantle convection at 108 Rayleigh number: Effects of depth-dependent viscosity, heating mode, and an endothermic phase change, *J. Geophys. Res.*, *102*, 11,991–12,007.

Busse, F. H. (1978), The optimum theory of turbulence, *Adv. Appl. Mech.*, *18*, 77–121.

Busse, F. H. (1985), Transitions to turbulence in Rayleigh-Bénard convection, in *Hydrodynamic Instabilities and the Transition to Turbulence*, edited by H. L. Swinney, and J. P. Gollub, pp. 97–137, Springer, New York.

Busse, F. H., M. A. Richards, and A. Lenardic (2006), A simple model of high Prandtl and high Rayleigh number convection bounded by thin low viscosity layers, *Geophys. J. Int.*, *164*, 160–167, doi:10.1111/j.1365-246X.2005.02836.x.

Craig, C. H., and D. P. McKenzie (1986), The existence of a thin low viscosity layer beneath the lithosphere, *Earth Planet. Sci. Lett.*, *78*, 420–426.

Davies, G. F., and M. A. Richards (1992), Mantle convection, *J. Geol*, *100*, 151–206.

Ekstrom, G., and A. M. Dziewonski (1998), The unique anisotropy of the Pacific upper mantle, *Nature*, *394*, 168–172.

Grigné, C., S. Labrosse, and P. J. Tackley (2005), Convective heat transfer as a function of wavelength: Implications for the cooling of the Earth, *J. Geophys. Res.*, *110*, B03409, doi:10.1029/2004JB003376.

Gutenberg, B. (1959), *Physics of the Earth's Interior*, Elsevier, New York.

Hager, B. H., and M. A. Richards (1989), Long-wavelength variations in the Earth's geoid: Physical models and dynamical implications, *Philos. Trans. R. Soc. London., Ser. A*, *328*, 309–327.

Hansen, U., D. A. Yuen, S. E. Kroening, and T. B. Larsen (1993), Dynamic consequences of depth-dependent thermal expansivity and viscosity on mantle circulations and thermal structure, *Phys. Earth Planet. Inter.*, *77*, 205–223.

Howard, L. N. (1972), Bounds on flow quantities, *Annu. Rev. Fluid Mech.*, *4*, 473–494.

Jaupart, C., and B. Parsons (1985), Convective instabilities in a variable viscosity fluid cooled from above, *Phys. Earth Planet. Inter.*, *39*, 14–32.

Karato, S., and H. Jung (1998), Water, partial melting and the origin of the seismic low velocity and high attenuation zone in the upper mantle, *Earth Planet. Sci. Lett.*, *157*, 193–207.

Kaula, W. M. (1990), Venus: A contrast in evolution to Earth, *Science*, *247*, 1191–1196.

Kiefer, W. S., M. A. Richards, B. H. Hager, and B. G. Bills (1986), A dynamic model of Venus' gravity field, *Geophys. Res. Lett.*, *13*, 14–17.

Lenardic, A., F. Nimmo, and L. Moresi (2004), Growth of the hemispheric dichotomy and the cessation of plate tectonics on Mars, *J. Geophys. Res.*, *109*, E02003, doi:10.1029/2003JE002172.

McGill, G. E., and A. M. Dimitriou (1990), Origin of the Martian global dichotomy by crustal thinning in the late Noachian or early Hesperian, *Geology*, *28*, 391–394.

Moresi, L.-N., and V. S. Solomatov (1995), Numerical investigations of 2D convection with extremely large viscosity variations, *Phys. Fluids*, *7*, 2154–2162.

Moresi, L.-N., and V. S. Solomatov (1998), Mantle convection with a brittle lithosphere: Thoughts on the global styles of the Earth and Venus, *Geophys. J. Int.*, *133*, 669–682.

Moresi, L.-N., S. J. Zhong, and M. Gurnis (1996), The accuracy of finite element solutions of Stokes' flow with strongly varying viscosity, *Phys. Earth Planet. Inter.*, *97*, 83–94.

Morris, S. J. S. (2003), Long-wave analysis of thermal convection with low-viscosity channels (abstract), *Bull. Am. Phys. Soc.*, *48*, 72.

Morris, S. J. S. (2005), Viscosity stratification and the aspect ratio of convection rolls (abstract), *Bull. Am. Phys. Soc.*, *50*, 143.

Nimmo, F., and D. Stevenson (2000), The influence of early plate tectonics on the thermal evolution and magnetic field of Mars, *J. Geophys. Res.*, *105*, 11,969–11,979.

Richards, M. A., W. Yang, J. R. Baumgardner, and H. Bunge (2001), Role of a low-viscosity zone in stabilizing plate tectonics: Implications for comparative terrestrial planetology, *Geochem. Geophys. Geosyst.*, *2*(8), doi:10.1029/2000GC000115.

Richards, M. A., S. Morris, F. Busse, and A. Lenardic (2003), Towards a physical understanding of the effects of depth-dependent rheology on mantle convection, *Eos. Trans. AGU*, *84*(46), Fall Meet. Suppl., Abstract S11G-06.

Richter, F. M., and S. F. Daly (1978), Convection models having a multiplicity of large horizontal scales, *J. Geophys. Res.*, *83*, 4951–4956.

Schubert, G., S. C. Solomon, D. L. Turcotte, M. J. Drake, and N. H. Sleep (1992), Origin and thermal evolution of Mars, in *Mars*, edited by H. H. Kieffer et al., pp. 147–183, Univ. of Ariz. Press, Tucson.

Sleep, N. H. (1994), Martian plate tectonics, *J. Geophys. Res.*, *99*, 5639–5655.

Solomatov, V. S. (1995), Scaling of temperature- and stress-dependent viscosity convection, *Phys. Fluids*, *7*, 266–274.

Stein, C., J. Schmalzl, and U. Hansen (2004), The effect of rheological parameters on plate behaviour in a self-consistent model of mantle convection, *Phys. Earth Planet. Inter.*, *142*, 225–255.

Stixrude, L., and C. Lithgow-Bertelloni (2005), Mineralogy and elasticity of the oceanic upper mantle: Origin of the low-velocity zone, *J. Geophys. Res.*, *110*, B03204, doi:10.1029/2004JB002965.

Su, W. J., and A. M. Dziewonski (1992), On the scales of mantle heterogeneity, *Phys. Earth Planet. Inter.*, *74*, 29–54.

Tackley, P. J. (1996a), Effects of strongly variable viscosity on three-dimensional compressible convection in planetary mantles, *J. Geophys. Res.*, *101*, 3311–3332.

Tackley, P. J. (1996b), On the ability of phase transitions and viscosity layering to induce long wavelength heterogeneity in the mantle, *Geophys. Res. Lett.*, *23*, 1985–1988.

Tackley, P. J. (1998), Self-consistent generation of tectonic plates in three-dimensional mantle convection, *Earth Planet. Sci. Lett.*, *157*, 9–22.

Tackley, P. J. (2000a), Self-consistent generation of tectonic plates in time-dependent, three-dimensional mantle convection simulations, *Geochem. Geophys. Geosyst.*, *1*(8), doi:10.1029/2000GC000036.

Tackley, P. J. (2000b), Self-consistent generation of tectonic plates in time-dependent, three-dimensional mantle convection simulations, *Geochem. Geophys. Geosyst.*, *1*(8), doi:10.1029/2000GC000043.

Thoraval, C., and M. A. Richards (1997), The geoid constraint in global geodynamics: viscosity structure, mantle heterogeneity models and boundary conditions, *Geophys. J. Int.*, *131*, 1–8.

Trompert, R., and U. Hansen (1998), Mantle convection simulations with rheologies that generate plate-like behavior, *Nature*, *395*, 686–689.

Turcotte, D. L. (1993), An episodic hypothesis for Venusian tectonics, *J. Geophys. Res.*, *98*, 17,061–17,068.

Turcotte, D. L., and E. R. Oxburgh (1967), Finite amplitude convection cells and continental drift, *J. Fluid Mech.*, *28*, 29–42.

Turcotte, D. L., and G. Schubert (1982), *Geodynamics: Applications of Continuum Physics to Geological Problems*, 450 pp., John Wiley, Hoboken, N. J.

Zhang, S. X., and D. A. Yuen (1995), The influences of lower mantle viscosity stratification on 3d spherical-shell mantle convection, *Earth Planet. Sci. Lett.*, *132*, 157–166.

Zhong, S., and M. T. Zuber (2001), Degree-1 mantle convection and the crustal dichotomy on Mars, *Earth Planet. Sci. Lett.*, *189*, 75–84.

Zhong, S., M. T. Zuber, L. Moresi, and M. Gurnis (2000), Role of temperature-dependent viscosity and surface plates in spherical shell models of mantle convections, *J. Geophys. Res.*, *105*, 11,063–11,082.

F. H. Busse, Institute of Physics, University of Bayreuth, D-95440, Bayreuth, Germany.

A. Lenardic, Department of Earth Science, MS 126, P.O. Box 1892, Rice University, Houston, TX 77251-1892, USA. (adrian@esci.rice.edu)

M. A. Richards, Department of Earth and Planetary Science, University of California, Berkeley, CA 94720-4767, USA. (markr@seismo.berkeley.edu)